Friction

Research Article

The implementation of the Johnson–Kendall–Roberts formalism on the basis of numerically simulated contact problems

Zhizhen Jiang[1], Feodor M. Borodich[1,✉], Nikolay V. Perepelkin[2,✉], Xiaoqing Jin[1]

Cite this article: Jiang ZZ, Borodich FM., Perepelkin NV, et al. *Friction* 2026, **14**(7): 9441226. https://doi.org/10.26599/FRICT.2026.9441226

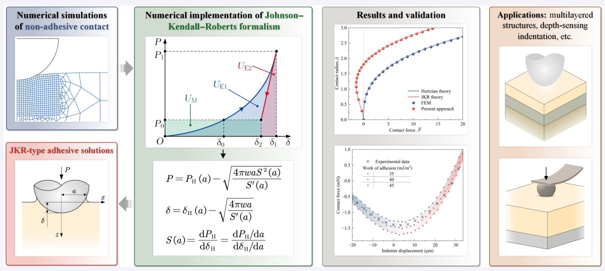

ABSTRACT: The Johnson–Kendall–Roberts (JKR) theory remains the most cited model of adhesive contact. It was demonstrated that the JKR theory can be substantially extended, allowing adhesive JKR-type contact problems to be solved through an explicit transformation of the corresponding nonadhesive Hertz-type load–displacement curve. This framework enables the application of the extended JKR theory to nonclassical scenarios where analytical nonadhesive solutions are unavailable, and therefore, numerical methods can be employed. However, the transformation formulae involve the first and second derivatives of the load–displacement curve, posing challenges when applied to discrete numerical data. This study presents a straightforward and effective numerical approach that converts a numerically obtained data series of load–displacement–contact radius for a nonadhesive contact problem into the corresponding JKR-type adhesive solution. While any appropriate numerical method can be used to generate these data, the finite element method (FEM) is employed here. The proposed approach is validated by comparing numerical results with established analytical solutions for adhesive contact problems involving an elastic half-space and a thin elastic layer bonded to a rigid substrate, as well as with experimental data. These comparisons demonstrate excellent agreement between the numerical and analytical solutions. It is argued that the proposed method offers significant potential for solving many important practical problems, e.g., adhesive contact analysis for coated or multilayered media.

KEYWORDS: adhesive contact; finite element method (FEM); Johnson–Kendall–Roberts (JKR) theory; load–displacement curves; depth-sensing indentation; work of adhesion

1 Introduction

Adhesive properties constitute one of the most crucial interfacial characteristics, particularly at the micro/nanoscale [1, 2]. As the characteristic size L of an object decreases, the surface area-to-volume ratio increases, causing surface energy ($\propto L^2$) to progressively dominate over stored elastic energy and volumetric forces ($\propto L^3$). This scaling relationship renders surface forces increasingly predominant in determining mechanical responses, significantly altering material performance through interfacial adhesion mechanisms [3].

The critical influence of adhesion can be observed across diverse engineering and scientific applications. For instance, in microelectromechanical systems (MEMS), minimizing adhesive forces could prevent stiction-induced device failures [4–6], while in biomimetic materials, optimizing adhesion is essential for designing effective bioinspired adhesive microstructures [7–9]. Furthermore, elucidating cellular and viral adhesion mechanisms can provide fundamental insights into biological processes [10]. Given this broad technological and scientific significance, developing comprehensive theoretical frameworks and robust methodologies for investigating adhesive behaviors represents an important research endeavor.

The mechanics of adhesive contact have evolved into a prominent scientific field, stemming from the pioneering foundational works of Derjaguin [11, 12]. The Derjaguin approximation, in particular, represents a cornerstone contribution that remains implicitly incorporated in various contemporary models of adhesive contact [13–16]. This approximation [11] simplifies intermolecular interactions between curved surfaces by converting volume forces into surface forces [17], considering only the closest surface elements along vertical straight lines and treating the curved surfaces locally as parallel planes to determine the interaction energy. Several widely used

[1] College of Aerospace Engineering, Chongqing University, Chongqing 400030, China. [2] School of Built Environment, Engineering and Computing, Leeds Beckett University, Leeds LS2 8AJ, UK.

✉ Corresponding authors. E-mail: F. Borodich, borodichfm@cqu.edu.cn; N. Perepelkin, n.perepelkin@leedsbeckett.ac.uk

Received: November 8, 2025; Revised: December 30, 2025; Accepted: January 27, 2026

analytical models for adhesive contact have been developed based on the Derjaguin approximation, most notably the Johnson–Kendall–Roberts (JKR) [18], Derjaguin–Muller–Toporov (DMT) [12, 19], and Maugis–Dugdale (M–D) models [20].

Generally, the JKR model is considered suitable for soft materials or strong adhesive interactions, whereas the DMT model applies more effectively to hard materials or weak adhesive interactions [21]. The M–D model provides an intermediate transition between these two theoretical frameworks. Although these three models employ distinct methodologies and assumptions, each has extensive applications and demonstrates validity within specific ranges of the Tabor parameter μ given by Eq. (1) [21, 22]:

$$\mu = \left(\frac{Rw^2}{E^{*2}z_0^3}\right)^{\frac{1}{3}} \tag{1}$$

where E^* and R are the reduced elastic modulus and the effective radius of the contacting bodies, respectively, w denotes the work of adhesion, and z_0 represents the interatomic equilibrium distance. However, these classical theories are constrained to adhesive contact problems involving spherical indenters and half-spaces, which inherently limit their broader applicability. Therefore, researchers have sought to expand the theoretical boundaries of classical theories through numerical methods to investigate more complex adhesive contact problems.

Various strategies have been developed to incorporate adhesive effects into finite element (FE) models. The most direct approaches involve custom solvers [23, 24] or user subroutines [25–27] that treat interaction forces as body forces while integrating potential functions such as Lennard-Jones (LJ) potentials during contact simulation. Building upon this foundation, many researchers have adopted nonlinear spring elements positioned between contact bodies to capture both attractive and repulsive interactions [28–30]. A more sophisticated alternative computes surface tractions directly from potential functions or analytical adhesion models, subsequently applying these calculated tractions to simulate adhesive contact behavior [31, 32]. Fracture mechanics-based methods have also been developed to obtain adhesive contact solutions through cohesive zone models [33, 34] or superposition of multiple simulation results [35–37]. Despite these advances, implementing adhesive effects in finite element frameworks could remain cumbersome, requiring specialized modeling procedures and considerable programming efforts.

Apart from the finite element method (FEM), other computational techniques, such as the boundary element method (BEM), have been actively developed for modeling both nonadhesive and adhesive contact, particularly in rough surface contact analysis [38–42]. The BEM reduces the dimensionality of contact problems from three-dimensional domains to two-dimensional surfaces, employing computational frameworks such as constrained conjugate gradient methods [38, 40] or biconjugate gradient stabilized methods [39] while utilizing fast Fourier transforms to enhance computational efficiency. Additionally, several numerical algorithms have been developed that combine the Hamaker summation of LJ potentials for adhesion with the Green's function method for elastic deformation [16, 43–45]. Nevertheless, these methodologies require intricate programming and may suffer from computational inefficiency [39]. Molecular dynamics (MD) simulations have emerged as an alternative approach for modeling adhesive contact at atomic scales [46–48]. Although MD simulations provide intuitive representations of interfacial interactions, such methods remain constrained by computational bottlenecks regarding system size and accessible time scales [49].

Compared to the above methods, the classical analytical solutions for adhesive contact problems are straightforward to implement but are only applicable under specific conditions. While existing numerical methods can address more complex adhesive contact situations, they typically present substantial implementation challenges. The question arises whether a method can be developed that combines the implementation simplicity of analytical solutions with the versatility of numerical techniques to further extend the scope of the classic theories.

In the present work, we focus on integrating JKR-type adhesion (the JKR formalism [13, 50]) with numerical simulations of nonadhesive contact problems. Specifically, this study presents a numerical approach that enables the direct transformation of numerical results from nonadhesive contact problems into corresponding adhesive contact solutions. Since adhesive forces may originate from various physical phenomena [7, 13, 51, 52] (e.g., van der Waals interactions, chemical bonding, surface contamination), the work of adhesion provides a convenient means of accounting for multiple phenomena integrally as a single numerical quantity. This allows the elegant JKR theory to be applied without explicitly modeling various physical interactions at the contact interface. The proposed approach may prove useful in experimental studies, such as the identification of material properties from depth-sensing indentation, where adhesion effects are significant but difficult to quantify a priori.

Additionally, the present approach serves as a postprocessing stage for contact simulations. Thus, JKR-type adhesion can be incorporated into nonadhesive results from arbitrary numerical contact simulations (e.g., using FEM or BEM), provided that the problem satisfies the assumptions of JKR theory. This enables the treatment of adhesion effects in computational frameworks where interatomic potentials or similar techniques are not readily available, challenging to implement due to software limitations, or prohibitively complex. In particular, the presentation herein demonstrates the transformation of FEM simulation results into corresponding JKR-type adhesive solutions. This approach requires only standard FEM simulations without specialized programming or complex modeling procedures, followed by relatively straightforward postprocessing.

The paper is organized as follows. In Section 2, the JKR formalism is briefly presented, including both the classical JKR model and an extended JKR theory. The extended theory provides formulae that enable the direct transformation of nonadhesive contact solutions to their adhesive counterparts for largely arbitrary axisymmetric problems. The practical application of these formulae in processing discrete FEM-generated data is presented in Section 3, along with a detailed explanation of the corresponding numerical workflow. Section 4 validates the proposed method against known analytical solutions to classical contact problems and presents a comparison with experimental data. Some discussions around the potential scope and use cases of the method are given in Section 5, while Section 6 presents the main conclusions.

2 The JKR formalism

In this section, the classical JKR theory is first revisited. Building upon its elegant formalism (e.g., the superposition of Hertz-type and Boussinesq-type solutions and the energy balance approach), an extended JKR theory is subsequently presented, which introduces explicit formulae for converting nonadhesive solutions into their adhesive counterparts. Such formulae are applicable to the vast majority of axisymmetric adhesive contact problems without requiring intricate derivations or solving energy balance equations.

2.1 Classical JKR theory

As one of the classical theories of adhesive contact, the JKR theory [18] was established by employing Derjaguin's approach to calculating the total energy of contacting solids [11, 12] and a geometrically linear formulation of the contact problem, thus allowing an ingenious combination of the Hertzian contact theory for two elastic spheres [53]:

$$a_{\mathrm{H}}=\left(\frac{3P_{\mathrm{H}}R}{4E^{*}}\right)^{\frac{1}{3}},\quad \delta_{\mathrm{H}}=\frac{a_{\mathrm{H}}^{2}}{R}=\left(\frac{9P_{\mathrm{H}}^{2}}{16RE^{*2}}\right)^{\frac{1}{3}} \tag{2}$$

and Boussinesq solution for a flat-ended cylindrical indenter [54]:

$$\delta_{\mathrm{B}}=\frac{P_{\mathrm{B}}}{2E^{*}a_{\mathrm{B}}} \tag{3}$$

Here, the subscripts H and B indicate variables associated with the Hertzian and Boussinesq solutions, respectively. In Eqs. (2) and (3), a denotes the contact radius, P is the applied load, and δ is the indentation depth; the reduced elastic modulus E^* and the effective radius of the spheres R are defined as Eq. (4):

$$\frac{1}{E^{*}}=\frac{1-(\nu^{+})^{2}}{E^{+}}+\frac{1-(\nu^{-})^{2}}{E^{-}},\quad \frac{1}{R}=\frac{1}{R^{+}}+\frac{1}{R^{-}} \tag{4}$$

where E is Young's modulus, ν represents the Poisson's ratio, and the subscripts "+" and "−" refer to the two bodies in contact with each other.

Generally, in the absence of surface attraction forces, when a rigid spherical indenter with radius R contacts a half-space under an applied load P_0, the contact radius a_0 can be determined by solving the Hertzian contact problem. However, the presence of adhesive forces would result in an equilibrium contact radius a_1 that exceeds a_0 for the same load P_0, as experimentally observed by Kendall and Roberts in approximately 1970 [1]. To address this issue, the classical JKR formalism assumes that the adhesive contact system reaches the actual state via two imaginary sequential steps, as illustrated in Fig. 1: (i) initially achieving a contact radius a_1 and an indentation depth δ_1 under a Hertzian load P_1 without considering adhesion and (ii) subsequently unloading from P_1 to the true external load P_0 while maintaining constant contact radius a_1 in the presence of adhesion forces. It is worth mentioning that the Boussinesq solution for a flat punch of radius a_1 is applicable in the latter unloading step.

Based on the superposition of Hertzian and Boussinesq contact problems, the total energy of the contact system U_{T} comprises four components and can be written as Eq. (5):

$$U_{\mathrm{T}}=U_{\mathrm{E}}-U_{\mathrm{M}}+U_{\mathrm{S}}=U_{\mathrm{E1}}-U_{\mathrm{E2}}-U_{\mathrm{M}}+U_{\mathrm{S}} \tag{5}$$

where U_{E}, U_{M}, and U_{S} represent the stored elastic energy, mechanical energy in the applied load P_0, and the surface energy, respectively. The elastic energy U_{E} can be formulated as the difference between the contributions associated with the loading OA (U_{E1}) and unloading AB (U_{E2}) branches, i.e., $U_{\mathrm{E}}=U_{\mathrm{E1}}-U_{\mathrm{E2}}$, as depicted in Fig. 1. The mechanical energy supplied by the applied load can be expressed as $U_{\mathrm{M}}=P_0\delta_2$. Regarding the surface energy U_{S}, its formulation considers only the adhesive interactions within the contact region; hence, $U_{\mathrm{S}}=-w\pi a_1^2$, where w denotes the work of adhesion, which relates to the adhesive properties of the material and is typically determined experimentally. From a general point of view, the work of adhesion equals the energy per unit area required to separate two parallel surfaces from equilibrium to an infinite distance [55].

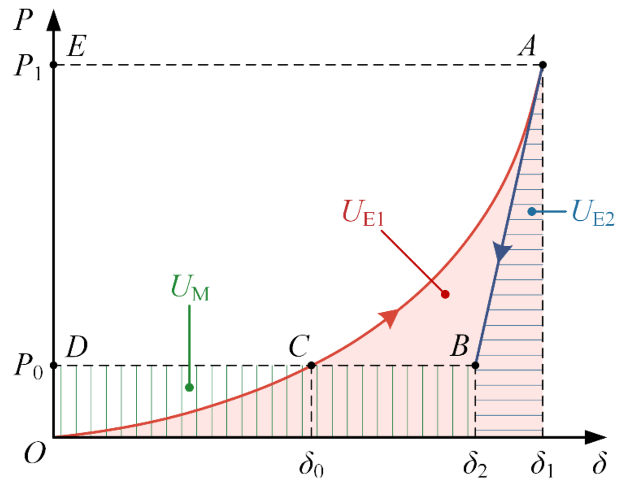

Fig. 1 An imaginary loading–unloading diagram elucidating the JKR theory. During the loading phase (branch OA), the load–displacement relationship follows the Hertzian contact relation $P\propto\delta^{3/2}$. The unloading phase (branch AB) exhibits a linear relationship consistent with the Boussinesq solution. The shaded regions represent distinct energy components of the system: U_{M} denotes the mechanical energy supplied by the applied load, while U_{E1} and U_{E2} represent the elastic energies for loading and unloading, respectively. The notations related to P and δ follow the classical work by Johnson et al. [18].

Based on Griffith's principle of energy balance, the derivative of the total energy is equal to zero in the equilibrium configuration, i.e.,

$$\frac{\mathrm{d}U_{\mathrm{T}}}{\mathrm{d}a_1}=0 \text{ or } \frac{\mathrm{d}U_{\mathrm{T}}}{\mathrm{d}P_1}=0 \tag{6}$$

This yields the well-known relations of classical JKR theory for adhesive contact, governing the applied load P_0, displacement δ_2, and contact radius a_1:

$$P_0=\frac{4E^{*}}{3R}a_1^3-\sqrt{8\pi wE^{*}a_1^3},\quad \delta_2=\frac{a_1^2}{R}-\sqrt{\frac{2\pi wa_1}{E^{*}}} \tag{7}$$

It is worthwhile to note that in 1964, Sperling [56] derived identical formulae to Eq. (7) except for the sign convention. Therefore, both JKR and JKRS (Johnson–Kendall–Roberts–Sperling) notations could be utilized in describing the theory of adhesive contact between elastic spheres [57].

2.2 Generalized JKR theory and transformation between nonadhesive and adhesive cases

The energy balance approach described above can be formulated in a more general form than originally proposed by Johnson et al. [18]. Following the classical JKR formalism, several researchers have attempted to develop relations directly linking Hertz-type nonadhesive and JKR-type adhesive contact problems [13, 50, 58, 59]. Among these contributions, Perepelkin and Borodich [50] conducted a systematic analysis and derived explicit transformation formulae applicable to largely arbitrary elastic systems using minimal initial assumptions. Following their approach, the key derivations are reformulated below for the present context.

Since different components of the total energy can be visualized as areas on the load–displacement diagram (Fig. 1), it becomes evident that when areas corresponding to positive and negative terms overlap, they eliminate each other. By identifying the overlapping areas among the regions representing U_{E1}, U_{E2}, and U_M, one can determine the remaining components of the total energy and express them mathematically. Accordingly, Eq. (5) can be rewritten as Eq. (8):

$$U_T = U_{CBA} - U_{OCD} + U_S \tag{8}$$

where the subscripts CBA and OCD represent the corner vertices of the remaining areas after elimination, as shown in Fig. 1. Equation (6) can now be applied in the form $\mathrm{d}U_T/\mathrm{d}P_1 = 0$. Note that as U_{OCD} depends on the actual external load P_0, which remains independent of variations in P_1, the differentiation of U_{OCD} with respect to P_1 identically yields zero, i.e., $\mathrm{d}U_{OCD}/\mathrm{d}P_1 = 0$.

For U_{CBA}, it is important to recognize that branch AB arises from employing the superposition of the flat punch solution corresponding to the true contact radius a_1 as the unloading path. This could be achieved by translating the line representing the Boussinesq solution by the distance $\delta_H(P_1) - \delta_B(a_1, P_1)$. Thus, $U_{CBA} = U_{DBAE} - U_{DCAE}$ can be further expressed as Eq. (9):

$$\begin{aligned} U_{CBA} &= \int_{P_0}^{P_1} \left(\delta_B(a_1,P) + \delta_H(P_1) - \delta_B(a_1,P_1) - \delta_H(P)\right)\mathrm{d}P \\ &= (P_1 - P_0)\left(\delta_H(P_1) - \delta_B(a_1,P_1)\right) + \\ &\quad \int_{P_0}^{P_1} \left(\delta_B(a_1,P) - \delta_H(P)\right)\mathrm{d}P \end{aligned} \tag{9}$$

Differentiating the above formula with respect to P_1 and considering $\mathrm{d}U_S/\mathrm{d}P_1 = -2\pi w a_1 (\mathrm{d}a_H(P_1)/\mathrm{d}P_1)$, the energy balance condition $\mathrm{d}U_T/\mathrm{d}P_1 = 0$ becomes

$$\begin{aligned} \frac{\mathrm{d}U_T}{\mathrm{d}P_1} = &\left[\int_{P_0}^{P_1} \frac{\partial \delta_B(a_1,P)}{\partial a_1}\mathrm{d}P - (P_1 - P_0)\frac{\partial \delta_B(a_1,P_1)}{\partial a_1} - 2\pi w a_1\right] \\ &\frac{\mathrm{d}a_H(P_1)}{\mathrm{d}P_1} + (P_1 - P_0)\left(\frac{\mathrm{d}\delta_H(P_1)}{\mathrm{d}P_1} - \frac{\partial \delta_B(a_1,P_1)}{\partial P_1}\right) = 0 \end{aligned} \tag{10}$$

This expression of energy balance can be further simplified under two conditions: (i) at any given value of the true contact radius, the load-displacement relations for the Hertz-type and Boussinesq-type problems exhibit identical slopes; (ii) the solution of the Boussinesq-type problem is linear with respect to both the indenter displacement and indentation force. Importantly, both conditions can be shown to be valid for a broad class of elastic media under reasonably general assumptions (including frictionless contact, validity of the superposition principle, and rotational symmetry) [50].

Denoting the slope as $S(a) = \mathrm{d}P/\mathrm{d}\delta$, the first condition can be expressed as $\mathrm{d}\delta_H/\mathrm{d}P_1 = \partial\delta_B(a_1,P_1)/\partial P_1 = 1/S(a_1)$, while the second becomes $\delta_B(a_1,P) = P/S(a_1)$, yielding $\partial\delta_B(a_1,P)/\partial a_1 = PS'(a_1)/S^2(a_1)$. Here, the prime denotes differentiation with respect to a_1. Substituting these expressions into Eq. (10) results in a simple relation:

$$\frac{(P_1 - P_0)^2}{2}\frac{S'(a_1)}{S^2(a_1)} = 2\pi w a_1 \tag{11}$$

which additionally assumes that $\mathrm{d}a_H(P_1)/\mathrm{d}P_1 \neq 0$. By taking into account the relations $(P_1 - P_0)/(\delta_1 - \delta_2) = S(a_1)$, $P_1 = P_H(a_1)$, and $\delta_1 = \delta_H(a_1)$, the above equation can be further derived into Eq. (12):

$$P_H(a_1) - P_0 = \sqrt{\frac{4\pi w a_1 S^2(a_1)}{S'(a_1)}},\quad \delta_H(a_1) - \delta_2 = \sqrt{\frac{4\pi w a_1}{S'(a_1)}} \tag{12}$$

To facilitate the comprehension and utilization of Eq. (12), the notations P_0, δ_2, and a_1 can be replaced with P, δ, and a, which denote the actual values of the total force, indenter displacement, and contact radius in the adhesive contact problem, respectively. Consequently, the following expressions can be obtained, which enable the explicit transformation of the solution to a broad class of axisymmetric nonadhesive contact problems into the corresponding JKR-type adhesive solutions without solving the equations of energy balance [13, 50]:

$$P = P_H(a) - \sqrt{\frac{4\pi w a S^2(a)}{S'(a)}},\quad \delta = \delta_H(a) - \sqrt{\frac{4\pi w a}{S'(a)}} \tag{13}$$

where the subscript H denotes the Hertz-type nonadhesive solution and

$$S(a) = \frac{\mathrm{d}P_H}{\mathrm{d}\delta_H} = \frac{\mathrm{d}P_H(a)/\mathrm{d}a}{\mathrm{d}\delta_H(a)/\mathrm{d}a} \tag{14}$$

represents the slope of the nonadhesive load-displacement curve. These relations can also be written in dimensionless form by introducing the normalization:

$$\bar{P} = \frac{P}{\pi w R},\quad \bar{\delta}^3 = \delta^3\frac{16E^{*2}}{9\pi^2 w^2 R},\quad \bar{a}^3 = a^3\frac{4E^*}{3\pi w R^2} \tag{15}$$

which reduces Eq. (13) to

$$\bar{P} = \bar{P}_H - 2\sqrt{\frac{\bar{a}\bar{S}^2(\bar{a})}{\bar{S}'(\bar{a})}},\quad \bar{\delta} = \bar{\delta}_H - 2\sqrt{\frac{\bar{a}}{\bar{S}'(\bar{a})}} \tag{16}$$

As a matter of fact, Eq. (13) represents not only a valuable extension of the classical JKR theory but also provides significant utility across numerous contact problems discussed in the literature, including indenters with power-law shapes [13, 60], toroidal indenters [61], isotropic [62, 63] or transversely isotropic layered structures [64], and stretched membranes such as graphene and other two-dimensional materials [65]. This explicit transformation allows one to obtain JKR-type adhesive solutions without intricate derivations or the need to solve energy balance equations as required by classical JKR theory. In other words, the classical JKR theory, represented by Eq. (7), addresses frictionless axisymmetric adhesive contact between a spherical indenter and an elastic half-space, whereas the extended JKR theory in Eq. (13) can be applied to axisymmetric adhesive contacts involving arbitrary convex indenters and elastic media that obey the superposition principle and exhibit rotational symmetry in elastic properties (i.e., isotropic or transversely isotropic materials) [13, 50]. Furthermore, unlike the classical JKR theory that relies on the specific mathematical forms of the Hertzian and Boussinesq solutions for a half-space, Eq. (13) relies on the energy balance condition and the superposition principle, independent of particular solution forms. Despite this generality, other complex cases involving different boundary conditions or geometric configurations (e.g., the problems of two-dimensional (2D) contact, particularly the contact of periodic 2D structures with grooves of waviness [66]) may require further theoretical development beyond the scope of the present work.

3 Numerical implementation of the JKR formalism

This section presents the numerical implementation of the generalized JKR theory given in Eq. (13). The implementation procedure is broadly applicable to discrete load-displacement data obtained from any appropriate numerical method, as the core computational steps remain independent of the specific approach used, aside from potential variations in initial data preprocessing. In brief, the process involves the following steps: Numerical simulations are performed to determine the Hertz-type nonadhesive contact force P_{H}, displacement δ_{H}, and contact radius a, from which $S(a)$ and its derivative $S'(a)$ are evaluated, and finally, the JKR-type adhesive contact solution is obtained by substituting these parameters into Eq. (13). The detailed procedures for each step are described subsequently.

In this work, the finite element method is employed as an illustrative example to generate numerical data for constructing JKR-type load-displacement curves. The proposed approach functions as a postprocessing stage following FEM simulation, which is a natural choice due to the wide availability of FE packages capable of simulating Hertz-type axisymmetric contact. For substrates with complex material properties or geometries (e.g., multilayered structures), deriving analytical solutions remains challenging or impossible for nonadhesive contact and presents even greater difficulties for adhesive contact. However, FEM simulations could readily provide numerical solutions for contact problems involving these complex configurations. Once these nonadhesive numerical results are obtained, the generalized JKR theory presented in Section 2.2, combined with its numerical implementation described herein, offers a straightforward and efficient pathway to derive the corresponding adhesive contact solution.

It should be noted that there have been other attempts to implement the JKR theory using the FEM, such as the work by Sridhar, Johnson, and collaborators [36, 37]. Their method involved FEM-based computation of dimensionless functions that served as correction factors to the standard JKR relations. This was achieved by interpreting the adhesive problem as a fracture mechanics problem, which required the computation of stress intensity factors and consequently entailed nontrivial and onerous processing of stress distributions in the FE model. In contrast, the method presented in this section enables the construction of the JKR solution based solely on the values of the total force, indenter displacement, and contact radius, which can be extracted from FEM results directly and then processed by custom code involving several simple steps as outlined below.

Figure 2 illustrates the flowchart of the numerical approach for constructing a JKR-type adhesive solution from a numerical data series. In the present work, these steps were implemented in a Python script utilizing the NumPy and SciPy packages, and FEM simulations were conducted with ABAQUS (2022) software in an axisymmetric configuration (2D FE model).

First, an axisymmetric contact simulation is performed using FEM. To enhance accuracy, optional enhancements, such as mesh refinements in the contact region and reduced load increments during the initial contact stage, can be employed. Following the contact simulation, a data extraction and preprocessing stage is conducted prior to determining $S(a)$ and $S'(a)$. This initial stage begins with extracting the contact force, indenter displacement, and contact radius from the simulation results. While the values of the indentation depth and force are straightforward to obtain from FEM simulations, determining the contact radius requires further consideration.

The values of the contact radius are determined by identifying the farthest contact node from the symmetry axis among those located on the contact interface and exhibiting the "slipping" status and then referring to the radial coordinates of this node in the undeformed configuration. This aligns with the geometrically linear assumptions of elasticity. In ABAQUS, this procedure for estimating the contact radius can be implemented through a simple Python script, as adopted in this study. It is worth mentioning that FE software packages can often directly provide values of the contact area. Based on the geometric relationship between the contact radius and contact area in axisymmetric contact for an indenter of a given shape (e.g., a sphere), the contact radius can also be readily calculated from the contact area, as shown in Appendix A. However, the reported values of the contact area may not always exhibit high accuracy and refer to the true deformed configuration, which does not fully align with the

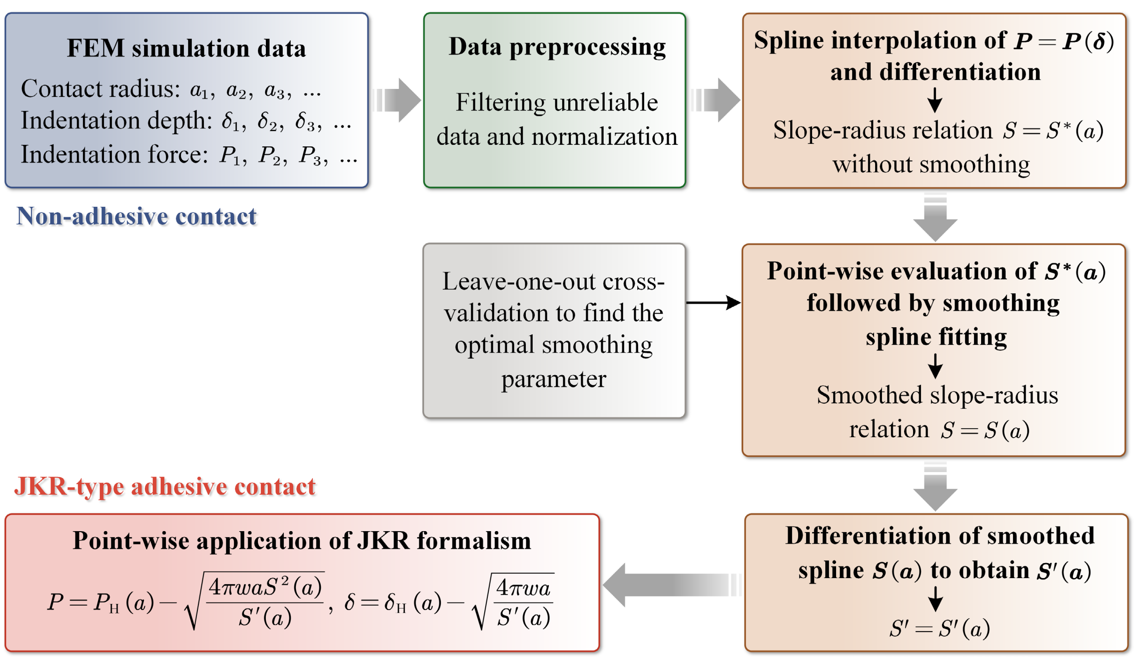

Fig. 2 Flowchart of the numerical implementation of JKR formalism. This framework converts discrete data points obtained from the numerical analysis of nonadhesive contact into its corresponding JKR-type adhesive solutions. The details of this workflow, including smoothing spline fitting and leave-one-out cross-validation, can be found in Appendix B.

assumptions of geometrically linear elasticity. Hence, this alternative method should be considered approximate despite its simplicity.

Due to the discrete nature of FE models, the accuracy and resolution of contact radius determination are constrained by the mesh size within the contact region, as the contact status is reported only at discrete nodes on the contact interface. This limitation causes the radial coordinate of the outermost contact node at the contact edge in FEM simulations to be typically smaller than the true contact radius that would occur on a continuous substrate. As the true contact radius increases with successive load increments, the outermost contact node may remain unchanged, thereby widening the discrepancy between the ideal contact radius and that estimated from FEM simulations. This phenomenon is illustrated in Fig. 3, which shows the true location of the contact boundary for consecutive load increments. As evident from the figure, multiple load increments may have the same contact boundary reported by FEM software (increments N, N+1, and N+2 in Fig. 3). Thus, the discrete nature of the FE model may result in apparently unchanged contact boundaries over multiple load increments, while the real boundary of the contact region expands continuously.

Accordingly, data extracted from FEM simulations require filtering based on the contact radius. When several consecutive load increments (i.e., FE timesteps) report the same outermost contact node, the first data point in such a sequence is the most accurate, while subsequent points are less reliable and need to be discarded. Specifically, only the data corresponding to the minimum contact force or displacement are retained for each sequence in which the same node serves as the outermost contact node. This filtering process eliminates unreliable data points and improves accuracy in subsequent analyses. Finally, the preprocessing of the FEM data is completed by transforming the results into dimensionless form using the scaling relations given in Eq. (15). The dimensionless contact force, displacement, and radius are thus produced as numerical arrays $\overline{P}_{\mathrm{H}}$, $\overline{\delta}_{\mathrm{H}}$, and $\overline{a}$.

After the preprocessing stage, the main processing stage begins. Cubic spline interpolation is applied to $\overline{P}_{\mathrm{H}}$ and $\overline{\delta}_{\mathrm{H}}$ to obtain smooth and continuous functions. The first derivative of the resulting cubic spline is then evaluated at the data points, with the additional constraint $\overline{S}(0)=0$ enforced to satisfy the theoretical slope of the load-displacement curve for a smooth indenter at initial contact. This constraint is necessary, as the computational noise and reduced accuracy in the FE data points at initial contact prevent $\overline{S}(0)=0$ from being exactly satisfied through the numerical procedure. These steps enable matching the values of the slope and contact radii, thereby constructing the dependency $\overline{S}(\overline{a})$.

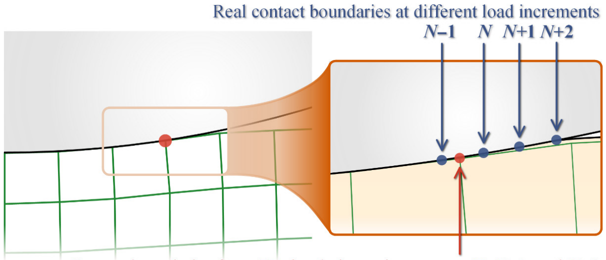

Fig. 3 The discrepancy between the boundaries of the contact region as reported in a finite element simulation and the real boundaries for an elastic continuum. Due to the discrete nature of finite element models, contact boundaries may appear unchanged across consecutive load increments, whereas the true contact boundaries for the equivalent ideal continuum expand continuously.

The slope values $\overline{S}(\overline{a})$ obtained in the previous step cannot be used directly to determine $\overline{S}'(\overline{a})$, as further differentiation significantly amplifies numerical inaccuracies in the data, particularly as $\overline{S}(\overline{a})$ already results from a differentiation step. Therefore, a data smoothing procedure needs to be applied to the derived $\overline{S}(\overline{a})$.

Recognizing the inherent errors in both the interpolation-derived derivative $\overline{S}(\overline{a})$ and the estimated contact radius, a smoothing spline is subsequently employed to fit the $\overline{S}(\overline{a})$ curve before calculating $\overline{S}'(\overline{a})$. This approach is meant to address issues arising from repeated differentiation of numerical data and boundary effects arising from the preceding steps, such as spline fitting. The smoothing spline is constructed as an augmented least-squares spline fitting problem, which incorporates a regularization term that penalizes the roughness in the fitting spline. The optimal smoothing parameter is determined automatically using leave-one-out cross-validation (LOOCV). Details regarding the formulation of smoothing splines and the LOOCV approach are provided in Appendix B.

Once the smoothing spline for the dependency $\overline{S}(\overline{a})$ is obtained, its first derivative is computed to yield $\overline{S}'(\overline{a})$. The values of $\overline{S}'(\overline{a})$ can then be accurately evaluated at each data point. As an optional step, the values of $\overline{S}(\overline{a})$ may also be re-evaluated using the smoothing spline; however, the examples below demonstrate high-quality approximations even without this additional step. Other modifications of the algorithm are possible, such as further smoothing the values of $\overline{S}'(\overline{a})$ when necessary.

Finally, substituting all the obtained values into the dimensionless form of Eq. (13) enables the transformation of $\overline{P}_{\mathrm{H}}$ and $\overline{\delta}_{\mathrm{H}}$ from nonadhesive to adhesive solutions. The results are naturally presented as discrete data points, consistent with the input data from FEM software. An appropriate smoothing or interpolation technique can be applied to obtain continuous curve representations. Note that the dimensionless expressions of Eq. (13) vary with different dimensionless schemes. For the contact problem involving a spherical indenter and a homogeneous half-space, the dimensionless variables in Eq. (15) may be employed, resulting in Eq. (16).

4 Results

This section presents the validation of the proposed methodology through comparison with established analytical solutions and experimental data. To demonstrate its accuracy and reliability, two classical contact problems are examined: contact between a rigid spherical indenter and (i) an elastic half-space and (ii) an elastic thin layer bonded to a rigid substrate. In each case, JKR-type adhesive contact solutions are obtained purely through numerical computation and systematically compared against known analytical solutions from the literature. Additionally, the numerical results are validated against experimental measurements to further establish the robustness of the approach.

As noted in Section 2.2, the proposed approach is applicable to a broad range of axisymmetric contact problems and is not limited to the two specific cases presented here. These cases were selected because they have been extensively studied and their analytical or asymptotic solutions are well known in the literature [18, 53, 62], enabling quantitative comparison between numerical results and reference solutions. Since the proposed approach is fundamentally based on the JKR formalism, the adhesive results are inherently JKR-type, making JKR-type analytical solutions suitable benchmarks for validation. There are no restrictions on the choice of finite element analysis software for FEM simulations or programming languages for data processing, including filtering and curve fitting. In this study, ABAQUS (2022) and Python were employed, as mentioned above.

4.1 Adhesive contact problem for a half-space

An axisymmetric FE model is established to describe the contact between a rigid spherical indenter with a radius R = 100 μm and an elastic substrate, as depicted in Fig. 4. The substrate is modeled as linearly elastic, homogeneous, and isotropic, characterized by Young's modulus (E = 5 GPa) and Poisson's ratio (ν = 0.4). The thickness H and radius L of the substrate are set to 20R and 12R, respectively, with the bottom surface fully constrained and the displacement of the left edge restricted in the horizontal direction. This substrate works reasonably well as an elastic half-space within a very small margin of error, and previous research has validated the adequacy of these dimensions and boundary conditions [67–69]. To ensure accurate results while maintaining computational efficiency, a local mesh refinement is performed near the initial contact point, and a coarse mesh is used elsewhere in the model. The typical element sizes are approximately 0.0005–0.02R, 0.02–0.05R, and 0.05–0.5R in zones I, II, and III, respectively. Further details regarding the influence of mesh size on the results are provided in Appendix C. Ultimately, the FE model contains 413,132 quadrilateral elements of type CAX4R and 1,467 linear triangular elements of type CAX3.

The rigid indenter is allowed solely vertical indentation with a maximum depth of 0.03R to ensure that the assumption of small deformation remains valid [69]. The reaction force P required to maintain static equilibrium is calculated throughout the indentation process by the software. The load increment is fixed at 0.01 of the maximum load. The FE model incorporates a frictionless, "hard" contact interaction defined as a surface-to-surface contact. The surface of the rigid indenter serves as the master surface, while the upper surface of the substrate is designated as the slave surface. In addition, the contact constraint enforcement method is defined as the direct method, which implements given pressure-overclosure behavior without approximation or augmentation iterations.

Employing the dimensionless forms of contact force P, displacement δ, and contact radius a in Eq. (15), the Hertzian theory yields

$$\overline{P}(\overline{a}) = \overline{a}^3,\ \overline{\delta}(\overline{a}) = \overline{a}^2 \tag{17}$$

while the classical JKR theory gives

$$\overline{P}(\overline{a}) = \overline{a}^3 - \sqrt{6\overline{a}^3},\ \overline{\delta}(\overline{a}) = \overline{a}^2 - \frac{2}{3}\sqrt{6\overline{a}} \tag{18}$$

The dimensionless results from analytical solutions, numerical FEM simulations, and the proposed numerical implementation of the JKR formalism are illustrated in Fig. 5. The JKR curves were evaluated for the value of the work of adhesion as w = 50 J/m². It should be noted that the proposed approach is not restricted to any specific value or range of work of adhesion. Since this approach is fundamentally based on the JKR formalism, the comparison with JKR-type analytical solutions remains valid regardless of the value of w. However, the work of adhesion can

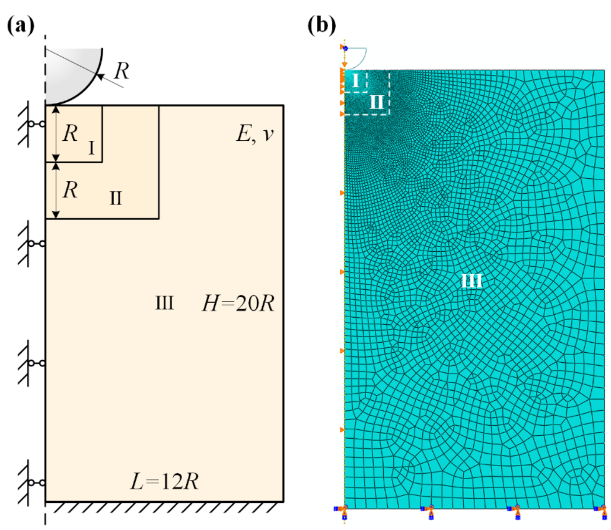

Fig. 4 (a) Schematic diagram of the axisymmetric finite element model featuring a rigid spherical indenter with radius R in contact with an elastic substrate with Young's modulus E, Poisson's ratio ν, thickness H = 20R, and radius L = 12R. The bottom surface of the substrate is fully constrained, and the displacement of the left edge is restricted in the horizontal direction. Zones I and II are square regions with side lengths of R and 2R, respectively. The scale has been adjusted for visual clarity. (b) Finite element model established in ABAQUS. Different mesh densities are applied within each zone.

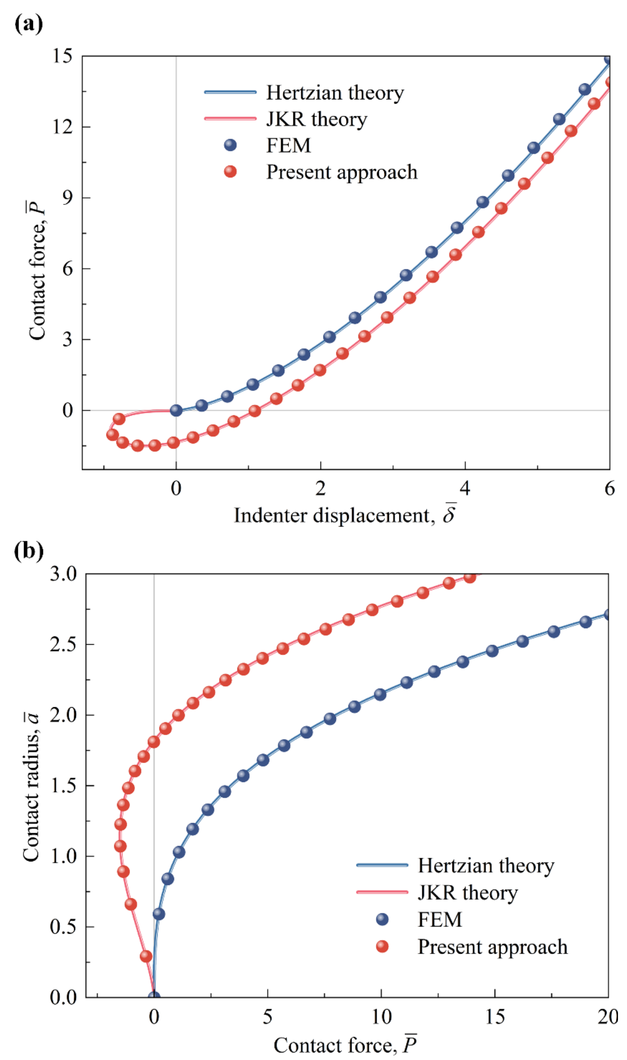

Fig. 5 Dimensionless results for half-space contact problems obtained through analytical solutions, finite element simulations, and the proposed numerical implementation of the JKR formalism: (a) load–displacement and (b) contact radius–force relationships.

influence the Tabor parameter, which is commonly used to assess the applicability of various continuum mechanics models. Assuming an interatomic equilibrium distance of 0.3 nm, which typically ranges from 0.2 to 0.4 nm for most materials, and applying Eq. (1), the corresponding Tabor parameter is calculated as $\mu \approx 639$, which is sufficiently large to justify the application of the JKR theory.

4.2 Adhesive contact problem for a thin elastic layer

For a rigid spherical indenter in contact with a thin elastic layer, an FE model was created using the same methodology described in Section 4.1, except for some modifications to specific geometrical parameters (Fig. 6). The substrate is modeled with a thickness of $h = 1$ μm and a radius $L = 30h$. The indenter radius is set to $1000h$, and the indenter displacement is prescribed as $0.15h$. The element size is defined as $0.02h$ within the contact region. The influence of mesh density on the results is discussed in Appendix C. The FE model comprises 75,000 linear quadrilateral elements of type CAX4R.

For contact problems involving a thin elastic layer bonded to a rigid substrate, with the thickness of the layer much smaller than the contact radius (i.e., $h \ll a$), asymptotic solutions exist for both nonadhesive and JKR-type adhesive cases [50, 62]. Using the Winkler–Fuss foundation [70, 71], which represents the isotropic or transversely isotropic layer as an equivalent spring system with stiffness K, and employing the dimensionless form of contact force P, displacement δ, and contact radius a:

$$\overline{P} = \frac{P}{2\pi wR}, \quad \overline{\delta}^2 = \delta^2 \frac{K}{2w}, \quad \overline{a}^4 = a^4 \frac{K}{8wR^2} \tag{19}$$

the leading-term asymptotic solutions can be obtained in the dimensionless form as

$$\overline{P}(\overline{a}) = \overline{a}^4, \quad \overline{\delta}(\overline{a}) = \overline{a}^2 \tag{20}$$

for nonadhesive contact problems of the thin layer, and as

$$\overline{P}(\overline{a}) = \overline{a}^4 - 2\overline{a}^2, \quad \overline{\delta}(\overline{a}) = \overline{a}^2 - 1 \tag{21}$$

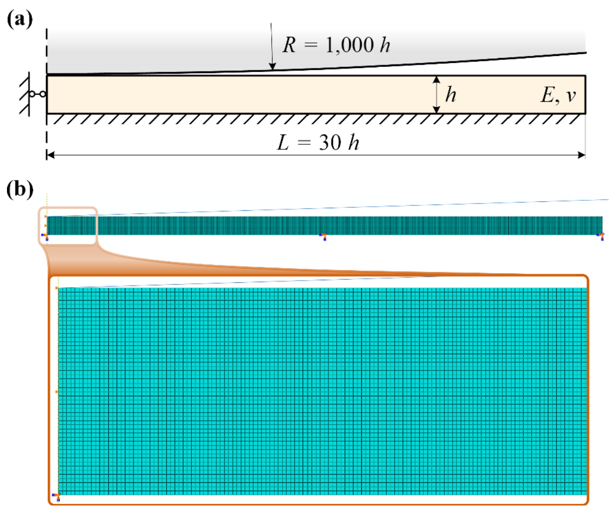

Fig. 6 (a) Schematic diagram of the axisymmetric finite element model featuring a rigid spherical indenter in contact with a thin elastic layer of thickness h and radius $L = 30h$. The layer has Young's modulus E and Poisson's ratio ν, while the indenter radius is $R = 1{,}000h$. Note that the scale has been adjusted for visual clarity. The bottom surface of the layer is fixed in all directions, and the left edge is constrained to prevent horizontal displacement. (b) Finite element model established in ABAQUS. The inset shows the uniform mesh size within the model.

for JKR-type adhesive contact of the thin layer. The stiffness K of the equivalent spring foundation representing a thin isotropic layer with thickness h, Young's modulus E, and Poisson's ratio ν is [72]:

$$K = \frac{E(1-\nu)}{h(1+\nu)(1-2\nu)} \tag{22}$$

Figure 7 presents the dimensionless results obtained from asymptotic solutions, numerical FEM simulations, and the proposed numerical approach, obtained with the work of adhesion set to 10 J/m². For reference, the Tabor parameter for an equivalent elastic half-space with identical material properties is $\mu \approx 471$, calculated using an interatomic equilibrium distance of 0.3 nm. The analytical solution employed here represents a leading-order asymptotic approximation that becomes increasingly accurate as the ratio of contact radius to layer thickness (a/h) approaches infinity [62]. The asymptotic approximation becomes less precise when the a/h ratio becomes finite. Nevertheless, from an overall perspective, both nonadhesive and adhesive solutions demonstrate good agreement between numerical and asymptotic results.

Consequently, the results presented in the above two sections

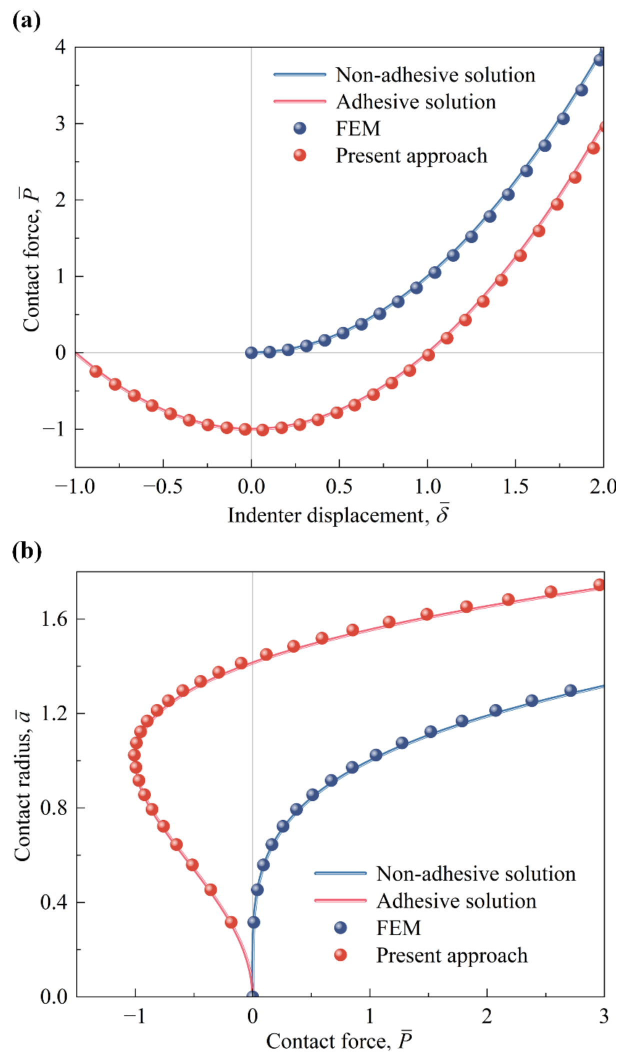

Fig. 7 Dimensionless results for contact problems of a thin layer obtained through asymptotic solutions, numerical finite element simulations, and the proposed numerical implementation of the JKR formalism: (a) load–displacement and (b) contact radius–force relationships.

show consistency with the JKR analytical solutions, confirming the validity of the proposed approach based on the JKR formalism.

4.3 Comparison with experimental results

To further demonstrate the effectiveness of the presented approach, the numerical results are compared with experimental data reported in Ref. [73]. In that study, a polydimethylsiloxane (PDMS)-coated glass sphere was indented into a thin gel layer. The FE simulations employed material and geometrical parameters consistent with those in Ref. [73]. Specifically, a rigid spherical indenter with a radius of 6 mm contacts a layer with a thickness of 0.36 mm, Young's modulus of 0.015 MPa, and Poisson's ratio of 0.499.

The comparison between the experimental and numerical results is presented in Fig. 8. Note that as the position of the zero point cannot be easily determined in indentation experiments [74], the experimental data shown in Fig. 8 are adjusted through horizontal translation after being extracted from Ref. [73]. It can be observed that the estimated work of adhesion ranges from 35 to 45 $\mathrm{mJ/m^2}$, which is consistent with the 30–60 $\mathrm{mJ/m^2}$ obtained from fracture mechanics analyses and empirical formulations [73].

5 Discussion

In this section, the practical advantages and applications of the proposed approach are discussed, with particular emphasis on the efficiency of its implementation and potential scope in nondestructive depth-sensing indentation (DSI) testing.

Although classical JKR theory is applicable only to axisymmetric contact problems, this limitation has not prevented its widespread use across various fields, including cellular biomechanics [75, 76], powder technology [77], and polymer engineering [78, 79]. The persistent emergence of new publications tagged "JKR theory" in scientometric databases indicates that the scientific community remains highly interested in this model, despite its axisymmetric configuration. While the approach presented in this work is also restricted to axisymmetric contact problems, the simplicity of implementing JKR theory becomes particularly valuable when the contact geometry is indeed axisymmetric. For instance, one important practical application where JKR theory proves particularly relevant is nondestructive material/specimen testing using DSI.

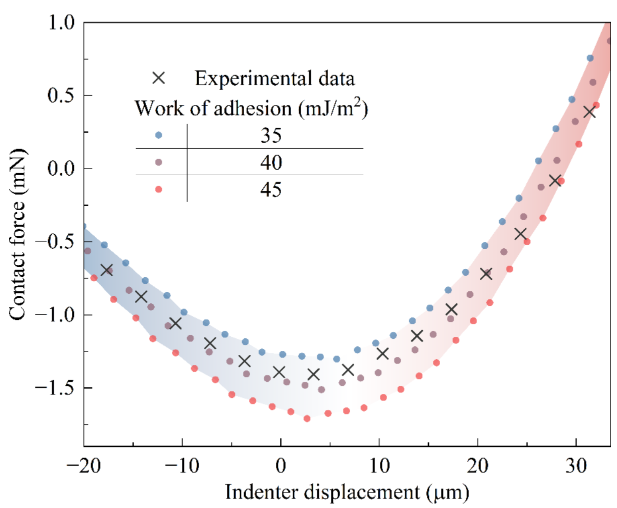

Fig. 8 Comparison of the experimental results with those obtained using the proposed numerical implementation of the JKR formalism. The experimental data are extracted from Ref. [73], with horizontal translation applied due to the indeterminate zero-point position inherent to indentation measurements.

When specimens are extremely small or available as thin coatings, DSI remains one of the few viable methods for determining their mechanical properties. The requirement for nondestructive testing may be critical for various reasons, including the examination of living specimens (from both practical and ethical perspectives), nondestructive quality control, or the need for repeated testing of the same specimen following exposure to external factors. Nondestructive DSI tests in such contexts can be performed using smooth (e.g., spherical) indenters; however, these experiments may be significantly affected by adhesive forces, particularly when indentation depths and forces are small. Hence, it becomes necessary to numerically estimate unknown adhesive interactions simultaneously with the unknown elastic moduli of the specimen, as adhesion can substantially impact such experiments. The experimental challenge described above can be addressed by the Borodich–Galanov (BG) method [80], which suggests conducting DSI tests with a smooth indenter and subsequently determining the unknown elastic and adhesive properties of the specimen by fitting experimental data to a mathematical model of the experiments (see the overview in Refs. [81, 82]). Experimental validation of this method has been reported in Ref. [74].

Essentially, in these experiments, one needs to take into account unknown adhesion in a quantitative manner. At the same time, when surface physics is not precisely known, detailed modeling of adhesion using interatomic potentials or other sophisticated methods is rarely feasible. Therefore, the work of adhesion can serve as a very convenient quantitative measure of adhesive effects in experiments, for instance, through the application of JKR theory where appropriate. Accordingly, the present approach establishes a foundation for material testing methods that account for adhesion, as the numerical implementation of the JKR formalism for such experiments can now be readily developed for nonclassical cases, such as finite-size specimens, layered specimens, and functionally graded transversely isotropic media.

It should be noted that several researchers have employed JKR theory in microscale DSI experiments, including the analysis of atomic force microscopy (AFM) indentation [83]. Notably, AFM probe tips may develop significant bluntness [84]; in such cases, the contact between the tip and substrate at small indentation depths can be considered a contact problem involving a smooth indenter with adhesion.

As discussed in Section 2.2, although the extended JKR theory has certain applicability limits, it remains valid for broad classes of axisymmetric contact problems; hence, the simplicity of the practical implementation of the present approach becomes a significant advantage. Compared with other numerical methods for solving adhesive contact problems, the proposed numerical approach eliminates the need for additional complex programming [23, 25, 39, 40], avoids cumbersome and unconventional finite element modeling procedures [28, 30, 85], and bypasses the tedious determination of strain energy release rates [35, 36]. In addition, the proposed approach requires only the work of adhesion as an input parameter to account for adhesion arising from multiple physical phenomena, thus conveniently incorporating adhesive effects without considering intermolecular potential functions. Furthermore, as a postprocessing technique applied to nonadhesive contact simulations, the method involves processing only the force–displacement–contact radius data series, consisting of a few dozen data points. The computational overhead is therefore negligible compared to the main simulation stage. Overall, the procedure described above represents an efficient and practical approach for obtaining adhesive contact solutions within the JKR formalism.

It is worth noting that the proposed approach enables JKR-type adhesion to be incorporated into results from various nonadhesive contact simulations, including those employing the FEM, BEM, or any other numerical schemes, provided that the conditions of the applicability of the JKR theory are satisfied. While FEM incorporated with intermolecular potentials can capture complex physical phenomena such as plasticity and contact jump-in/jump-out behavior [28, 29, 86], and BEM is well suited for adhesive contact problems involving rough surfaces [39, 40], the selection of the modeling approach should be guided by specific research objectives and practical constraints.

Different research contexts may benefit from different levels of modeling complexity, balancing accuracy requirements with computational efficiency and practical feasibility. For instance, in the indentation testing experiments discussed above, adhesive effects may be present and need to be considered, but the primary research objective is typically to measure material mechanical properties rather than to investigate adhesion mechanisms in detail. The proposed method provides distinct advantages for axisymmetric contact scenarios and efficiently incorporates adhesive effects without requiring detailed adhesion modeling. Given that each numerical approach has its own strengths and optimal application domains, the proposed method serves as a complement to existing tools for adhesive contact analysis.

6 Conclusions

This study presents a simple, straightforward, and effective numerical approach that allows the direct transformation of discrete data series obtained from a numerical simulation of a nonadhesive axisymmetric contact problem (indentation force, indentation depth, contact radius) into the respective JKR adhesive data series. The process is based on the numerical implementation of the explicit formulae of the JKR formalism, which allows the connection between the two kinds of problems (nonadhesive to adhesive).

The method works as a postprocessing stage for a nonadhesive numerical simulation of contact, and hence, it can be used to complement any such procedure, including FEM, BEM, and others, provided the conditions of the applicability of the JKR theory are satisfied. The methodology is explained here for the case when a nonadhesive contact problem is simulated in finite element software. The process includes initial data filtering, interpolation steps, and the use of smoothing splines to prevent the magnification of numerical noise that may be present in FE results used as input to the numerical procedure.

The validation cases for this method were the contact between a rigid punch and an elastic half-space and the contact between a punch and a thin layer bonded to a rigid base. These test cases, on the basis of well-established classical problems of contact mechanics, demonstrate the high accuracy of the proposed approach, as the processed FEM data are converted into JKR data and compared against the known analytical solutions. The two sets of results demonstrated excellent agreement. The approach can be extended to investigate a range of problems involving more complex structures, such as coated and multilayer systems, finite-thickness layers, finite-size models, etc. Additionally, integration with the BG method [74, 80] may enable the simultaneous determination of both the work of adhesion and effective Young's modulus from depth-sensing indentation experiments.

Appendix A

The relationship between the contact radius a and contact area A in the case of an axisymmetric indenter can be derived analytically. The contact between a rigid spherical indenter and an elastic substrate is considered here as an example. As illustrated in Fig. 9, the contact radius can be determined by solving

$$A = \int_0^{\varphi} 2\pi R \sin\theta \cdot R\mathrm{d}\theta = 2\pi R^2 \int_0^{\varphi} \sin\theta \mathrm{d}\theta \tag{A1}$$

where $\varphi = \arcsin(a/R)$. Note that $\cos(\arcsin(x)) = \sqrt{1-x^2}$, and Eq. (A1) can be further derived as

$$A = 2\pi R^2 \left[1 - \sqrt{1 - \left(\frac{a}{R}\right)^2}\right] \tag{A2}$$

Therefore, the contact radius can be calculated directly from the contact area using

$$a = \frac{\sqrt{(4\pi R^2 - A)A}}{2\pi R} \tag{A3}$$

Appendix B

Some details of the numerical procedure described in Section 3, including smoothing spline fitting and leave-one-out cross-validation, are presented here. The procedure can be implemented using various programming languages, such as Python or MATLAB. In the present study, the SciPy package was used for spline interpolation and fitting. The function scipy.interpolate.CubicSpline with the "not-a-knot" boundary condition was applied for cubic spline interpolation, while the function scipy.interpolate.make_smoothing_spline was recommended for smoothing spline fitting.

A smoothing spline [87, 88] is an optimal cubic spline function $f(x)$ that minimizes the penalized residual sum of squares by solving the following weighted regression problem:

$$\mathrm{RSS}(f,\lambda) = \sum_{i=1}^{n} w_i (y_i - f(x_i))^2 + \lambda \int_{x_1}^{x_n} (f''(u))^2 \mathrm{d}u \tag{B1}$$

where w_i represents a vector of weights and λ denotes a fixed smoothing parameter. The first term in Eq. (B1) quantifies data fidelity, while the second term penalizes the roughness in the function, with λ establishing a tradeoff between these two competing objectives. Larger values of λ yield smoother functions, while $\lambda = 0$ results in the interpolation of all data points. In this work, the weights w_i are chosen to enforce the theoretically expected condition $\bar{S}(0) = 0$ as follows. The very first element in the vector of weights is assigned a very large value, whereas the other elements have the value of 1. Hence, the smoothing spline will satisfy $\bar{S}(0) = 0$ nearly exactly.

The LOOCV approach is employed to determine the optimal smoothing parameter λ automatically. LOOCV solves the problem (spline fitting, in this case) on all data points except one, which serves as the test point and iterates through all points sequentially. The mean squared error (MSE) evaluates the performance of each smoothing parameter value, with the parameter yielding minimum MSE selected as optimal. For large datasets, generalized cross-validation [87, 88] could be utilized for efficient parameter selection.

Appendix C

For the presented approach, the effects of mesh size within the contact region in the FE models on the contact radius

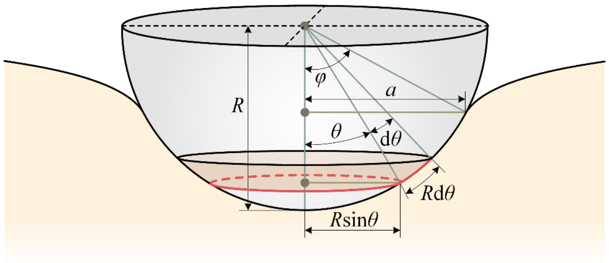

Fig. 9 Geometric relationship between contact radius and contact area for a rigid spherical indenter. R represents the radius of the spherical indenter, and a denotes the contact radius.

determination and the obtained numerical adhesive results are discussed here. In FE simulations of contact problems, mesh refinement of the contact region is essential to enhance simulation accuracy. Furthermore, in the present study, the mesh density can affect the accuracy of contact radius determination, which subsequently influences the density of discrete data points during processing and ultimately affects the transformed adhesive contact results (see Section 3 for details). For the two validation examples in Sections 4.1 and 4.2, different mesh densities within the contact region were employed, and the determined contact radii and obtained adhesive load-displacement results are illustrated in Fig. 10.

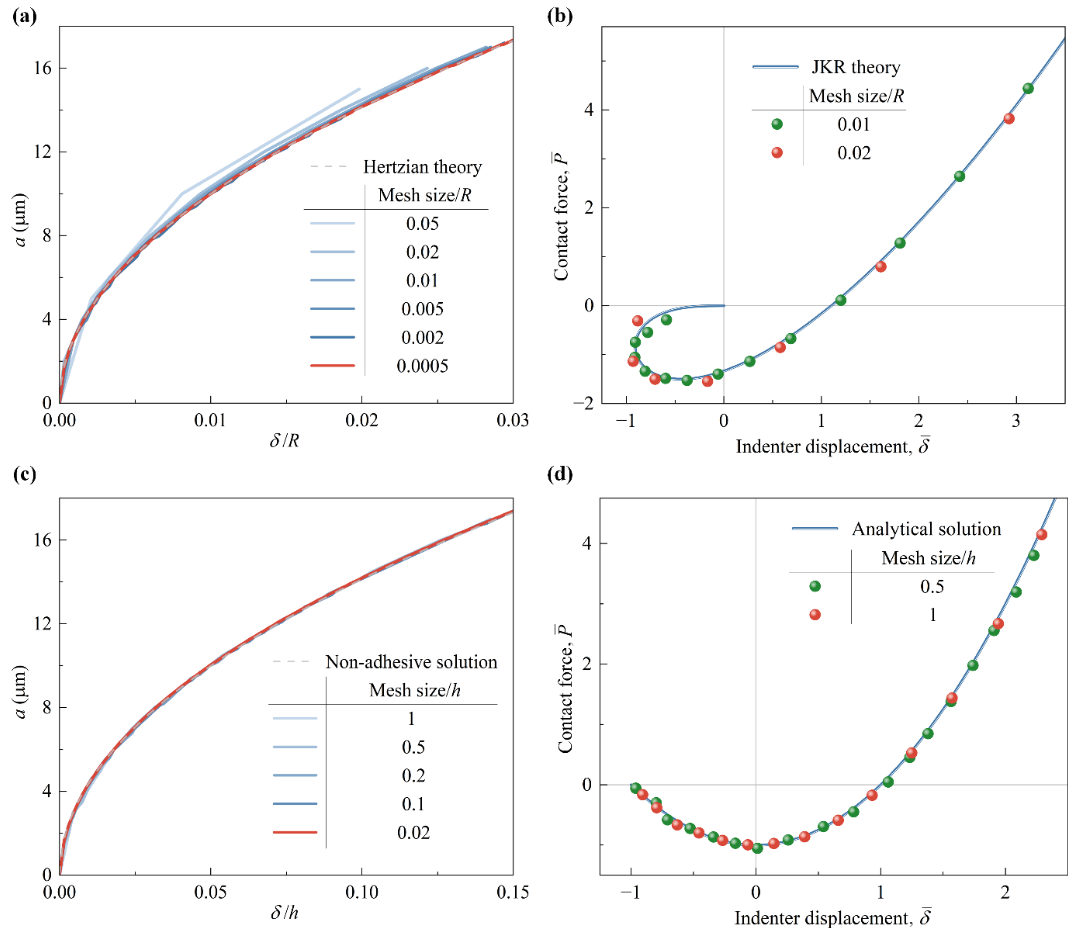

Fig. 10 Contact radius and obtained adhesive load-displacement results based on FE models with different mesh sizes in the contact region. (a) and (b) correspond to the half-space case (Section 4.1), and (c) and (d) correspond to the thin layer case (Section 4.2). The red lines in (a) and (c) indicate the mesh size adopted in the validation examples in Sections 4.1 and 4.2, respectively.

Figures 10(a) and 10(c) indicate that the mesh size adopted in the validation examples of Sections 4.1 and 4.2 is sufficient, as the determined contact radius remains basically unchanged when the mesh density is further increased. As the mesh size becomes larger, more data points could share the same outermost contact node. Consequently, a larger amount of data is filtered, as discussed in Section 3, resulting in fewer effective data points after preprocessing (Figs. 10(a) and 10(b)). The obtained adhesive load-displacement results for the half-space and thin layer cases based on FE simulation with coarse mesh density are presented in Figs. 10(b) and 10(d), respectively. These results exhibit good agreement with the analytical solutions, with only minor discrepancies in the initial portion of the curves. For better illustration, a finer mesh was adopted in the validations in Sections 4.1 and 4.2. The results presented in Figs. 10(b) and 10(d) demonstrate the robustness and effectiveness of the presented approach, as relatively coarse mesh densities can still yield reasonably accurate results while significantly reducing simulation time.

Acknowledgements

This work is supported by the National Natural Science Foundation of China (Nos. 52575201 and HWG2022001) and the Chongqing City Science and Technology Program (Nos. CSTB2025NSCQ-GPX0784 and CSTB2025NSCQ-GPX0778). Xiaoqing Jin would also like to acknowledge the Opening Fund of the State Key Laboratory of Nonlinear Mechanics (Institute of Mechanics, Chinese Academy of Sciences, China).

Availability of data and materials

The data that support the findings of this study are available from the corresponding author upon reasonable request.

Author contributions

Zhizhen Jiang: data curation, formal analysis, investigation, methodology, software, validation, visualization, writing—original draft; Feodor M. Borodich: conceptualization, methodology, writing—review & editing, supervision, funding acquisition; Nikolay V. Perepelkin: conceptualization, data curation, methodology, software, validation, writing—review & editing; Xiaoqing Jin: writing—review & editing, funding acquisition.

Declaration of competing interest

The authors have no competing interests to declare that are relevant to the content of this article.

References

[1] Kendall K. *Molecular Adhesion and Its Applications: The Sticky Universe*. New York (USA): Springer, 2001.

[2] Popov V L, Li Q, Lyashenko I A. Contact mechanics and friction: Role of adhesion. *Friction* **13**(1): 9440964 (2025)

[3] Borodich F M, Jin X Q, Eds. *Contact Problems for Soft, Biological and Bioinspired Materials*. Cham (Switzerland): Springer International Publishing, 2022.

[4] Zhao Y P, Wang L S, Yu T X. Mechanics of adhesion in MEMS: A review. *J Adhes Sci Technol* **17**(4): 519–546 (2003)

[5] Almuramady N, Borodich F M, Goryacheva I G, Torskaya E V. Damage of functionalized self-assembly monomolecular layers applied to silicon microgear MEMS. *Tribol Int* **129**: 202–213 (2019)

[6] Li H, Dai Z H. Adhesion of elastic microbeams on thin deformable substrates. *Eng Fract Mech* **313**: 110634 (2025)

[7] Heepe L, Gorb S N. Biologically inspired mushroom-shaped adhesive microstructures. *Annu Rev Mater Res* **44**: 173–203 (2014)

[8] Cheng Q, Borodich F M, Gao Z D, Gorb S N, Jin X Q. Advances in the contact mechanics theory and applications of biomimetic artificial adhesives inspired by biological multiscale hierarchical structures. *Friction* **13**(11): 9441016 (2025)

[9] Linghu C H, Liu Y, Yang X D, Li D, Tan Y Y, Mohamed Hafiz M H B, Rohani M F B, Du Z H, Su J T, Li Y, et al. Fibrillar adhesives with unprecedented adhesion strength, switchability and scalability. *Natl Sci Rev* **11**(10): nwae106 (2024)

[10] Kendall K, Kendall M, Rehfeldt F. *Adhesion of Cells, Viruses and Nanoparticles*. Dordrecht (the Netherlands): Springer, 2011.

[11] Derjaguin B. Friction and adhesion. IV. The theory of adhesion of small particles. *Kolloid Z* **69**(2): 155–164 (1934) (in German)

[12] Deryagin B V, Krotova N A, Smilga V P. *Adhesion of Solids*. New York (USA): Springer, 1978.

[13] Borodich F M. The Hertz-type and adhesive contact problems for depth-sensing indentation. *Adv Appl Mech* **47**: 225–366 (2014)

[14] Maugis D. *Contact, Adhesion and Rupture of Elastic Solids*. Heidelberg (Germany): Springer, 2000

[15] Zhu Y D, Ni Y, Huang C G, Yu J L, Yao H M, Zheng Z J. Unified model for adhesive contact between solid surfaces at micro/nano-scale. *J Mech Phys Solids* **196**: 106004 (2025)

[16] Tang X F, Yang W Y, Liang Y Y, Yang Q. Modeling adhesive contact behavior with interfacial displacement discontinuities. *Tribol Int* **210**: 110749 (2025)

[17] Bradley R S. *The cohesive force between solid surfaces and the surface energy of solids. Lond Edinb Dublin Philos Mag J Sci* **13**(86): 853–862 (1932)

[18] Johnson K L, Kendall K, Roberts A D. Surface energy and the contact of elastic solids. *Proc R Soc Lon Ser-A* **324**(1558): 301–313 (1971)

[19] Derjaguin B V, Muller V M, Toporov Y P. Effect of contact deformations on the adhesion of particles. *J Colloid Interf Sci* **53**(2): 314–326 (1975)

[20] Maugis D. Adhesion of spheres: The JKR-DMT transition using a dugdale model. *J Colloid Interf Sci* **150**(1): 243–269 (1992)

[21] Tabor D. Surface forces and surface interactions. *J Colloid Interf Sci* **58**(1): 2–13 (1977)

[22] Johnson K L, Greenwood J A. An adhesion map for the contact of elastic spheres. *J Colloid Interf Sci* **192**(2): 326–333 (1997)

[23] Sauer R A, Li S F. An atomic interaction-based continuum model for adhesive contact mechanics. *Finite Elem Anal Des* **43**(5): 384–396 (2007)

[24] Mergel J C, Scheibert J, Sauer R A. Contact with coupled adhesion and friction: Computational framework, applications, and new insights. *J Mech Phys Solids* **146**: 104194 (2021)

[25] Cho S S, Park S. Finite element modeling of adhesive contact using molecular potential. *Tribol Int* **37**(9): 763–769 (2004)

[26] Zhu X, Xu W. The effect of bottom boundary condition type on the behavior of adhesive contact of spherical probe on an elastic film. *J Phys D Appl Phys* **50**(46): 465305 (2017)

[27] Bortoleto E M, Prados E F, Seriacopi V, Fukumasu N K, da S Lima L G D B, Machado I F, Souza R M. Numerical modeling of adhesion and adhesive failure during unidirectional contact between metallic surfaces. *Friction* **4**(3): 217–227 (2016)

[28] Afferrante L, Violano G. On the effective surface energy in viscoelastic Hertzian contacts. *J Mech Phys Solids* **158**: 104669 (2022)

[29] Kadin Y, Kligerman Y, Etsion I. Loading–unloading of an elastic–plastic adhesive spherical microcontact. *J Colloid Interf Sci* **321**(1): 242–250 (2008)

[30] Luo J C, Liu J H, Xia H X, Ao X H, Fu Z H, Ni J, Huang H. Finite element analysis of adhesive contact behaviors in elastoplastic and viscoelastic media. *Tribol Lett* **72**: 7 (2024)

[31] Yang H D, Green I. Adhesion modelling by finite elements of three-dimensional fretting. *Tribol Int* **156**: 106802 (2021)

[32] Du Y, Chen L, McGruer N E, Adams G G, Etsion I. A finite element model of loading and unloading of an asperity contact with adhesion and plasticity. *J Colloid Interf Sci* **312**(2): 522–528 (2007)

[33] Zhao D W, Letz S, Jank M, März M. Adhesion strength of ductile thin film determined by cross-sectional nanoindentation. *Int J Mech Sci* **270**: 109103 (2024)

[34] Shen J H, He Z X, Chen H, Yang Y H, Jiang H Y. Exploiting interfacial instability during peeling a flexible plate from elastic films. *J Mech Phys Solids* **192**: 105821 (2024)

[35] Sridhar I, Zheng Z W, Johnson K L. A detailed analysis of adhesion mechanics between a compliant elastic coating and a spherical probe. *J Phys D Appl Phys* **37**(20): 2886–2895 (2004)

[36] Sridhar I, Johnson K L, Fleck N A. Adhesion mechanics of the surface force apparatus. *J Phys D Appl Phys* **30**(12): 1710–1719 (1997)

[37] Sridhar I, Zheng Z W. Effect of friction and adhesion on the load–displacement of a spherical probe in contact with a compliant incompressible elastic coating. *Tribol Int* **40**(2): 180–187 (2007)

[38] Rey V, Anciaux G, Molinari J F. Normal adhesive contact on rough surfaces: Efficient algorithm for FFT-based BEM resolution. *Comput Mech* **60**(1): 69–81 (2017)

[39] Wu J J. Numerical simulation on the adhesive contact between rough surfaces with bi-conjugate gradient stabilized method. *Tribol Lett* **65**(4): 151 (2017)

[40] Bugnicourt R, Sainsot P, Dureisseix D, Gauthier C, Lubrecht A A. FFT-based methods for solving a rough adhesive contact: Description and convergence study. *Tribol Lett* **66**: 29 (2018)

[41] Chen Y, Zhang M Q, Wang Q J. Analysis of adhesive contact of heterogeneous elastic materials. *Int J Mech Sci* **266**: 108986 (2024)

[42] Santeramo M, Carbone G, Krenn S, Putignano C. A novel energy-based numerical approach for adhesive contact mechanics of rough surfaces. *J Mech Phys Solids* **203**: 106217 (2025)

[43] Zhang Y Y, Wang X L, Li H Q, Wang B. Adhesive behavior of micro/nano-textured surfaces. *Appl Surf Sci* **329**: 174–183 (2015)

[44] Yang W X, Wang X L, Li H Q, Wu J, Hu Y Q, Li Z H, Liu H. Fundamental research on the effective contact area of micro-/nano-

textured surface in triboelectric nanogenerator. *Nano Energy* **57**: 41–47 (2019)
[45] Tang X F, Yang W Y, Yang Q, Liang Y Y. Effects of interfacial imperfections on nanoscale adhesive contact for layered medium. *Appl Math Model* **138**: 115803 (2025)
[46] Song J, Srolovitz D J. Adhesion effects in material transfer in mechanical contacts. *Acta Mater* **54**(19): 5305–5312 (2006)
[47] Si L N, Wang X L, Xie G X, Sun N. Nano-adhesion and friction of multi-asperity contact: A molecular dynamics simulation study. *Surf Interface Anal* **47**(9): 919–925 (2015)
[48] Zhao H H, Zhang L C, Gain A K, Li Z. Predicting the mold-glass interface adhesion in thermal molding. *Int J Mech Sci* **294**: 110265 (2025)
[49] Yuan X B, Zhao P Z, Fan Q Q. The peeling behavior of compliant nano-films in adhesive contact with a planar rigid substrate: Insights from molecular dynamics and continuum mechanics. *Thin Wall Struct* **204**: 112272 (2024)
[50] Perepelkin N V, Borodich F M. Explicit transformation between non-adhesive and adhesive contact problems by means of the classical Johnson–Kendall–Roberts formalism. *Philos T R Soc A* **379**(2203): 20200374 (2021)
[51] Xu Y, Wu S, Zhu Y D, Wu J. An adhesion model for contact electrification. *Int J Mech Sci* **272**: 109280 (2024)
[52] Yu C L, Dai Z H. Premature jump-to-contact with elastic surfaces. *J Mech Phys Solids* **193**: 105919 (2024)
[53] Hertz H. On the contact of elastic solids. *J Reine Angew Math* **92**: 156–171 (1881) (in German)
[54] Boussinesq J. *Applications of Potentials to the Study of the Equilibrium and Motion of Elastic Solids*. Paris (France): Gauthier-Villars, 1885 (in French)
[55] Israelachvili J N. *Intermolecular and Surface Forces*, 3rd edn. San Diego (USA): Academic Press, 2011.
[56] Sperling G. Theory of the Adhesion of Solid Particles to Solid Bodies. Ph.D. Thesis. Karlsruhe (Germany): Technische Hochschule Karlsruhe, 1964 (in German)
[57] Johnson K L, Pollock H M. The role of adhesion in the impact of elastic spheres. *J Adhes Sci Technol* **8**(11): 1323–1332 (1994)
[58] Shull K R. Contact mechanics and the adhesion of soft solids. *Mater Sci Eng R Rep* **36**(1): 1–45 (2002)
[59] Popov V L. Solution of adhesive contact problem on the basis of the known solution for non-adhesive one. *FU Mech Eng* **16**(1): 93–98 (2018)
[60] Borodich F M, Galanov B A, Suarez-Alvarez M M. The JKR-type adhesive contact problems for power-law shaped axisymmetric punches. *J Mech Phys Solids* **68**: 14–32 (2014)
[61] Argatov I, Li Q, Pohrt R, Popov V L. Johnson–Kendall–Roberts adhesive contact for a toroidal indenter. *P Roy Soc A* **472**(2191): 20160218 (2016)
[62] Borodich F M, Galanov B A, Perepelkin N V, Prikazchikov D A. Adhesive contact problems for a thin elastic layer: Asymptotic analysis and the JKR theory. *Math Mech Solids* **24**(5): 1405–1424 (2019)
[63] Erbaş B, Aydın Y E, Borodich F M. Indentation of thin elastic films glued to rigid substrate: Asymptotic solutions and effects of adhesion. *Thin Solid Films* **683**: 135–143 (2019)
[64] Argatov I I, Borodich F M, Popov V L. JKR adhesive contact for a transversely isotropic layer of finite thickness. *J Phys D Appl Phys* **49**(4): 045307 (2016)
[65] Borodich F M, Galanov B A. Contact probing of stretched membranes and adhesive interactions: Graphene and other two-dimensional materials. *P Roy Soc Lond A Mat* **472**(2195): 20160550 (2016)
[66] Menga N, Afferrante L, Carbone G. Adhesive and adhesiveless contact mechanics of elastic layers on slightly wavy rigid substrates. *Int J Solids Struct* **88–89**: 101–109 (2016)
[67] Du Y K, Stewart P, Hill N A, Yin H B, Penta R, Köry J, Luo X Y, Ogden R. Nonlinear indentation of second-order hyperelastic materials. *J Mech Phys Solids* **171**: 105139 (2023)
[68] Guo Z Y, Hao M R, Jiang L, Li D F, Chen Y, Dong L T. A modified Hertz model for finite spherical indentation inspired by numerical simulations. *Eur J Mech A-solids* **83**: 104042 (2020)
[69] Wu C N, Lin K H, Juang J Y. Hertzian load–displacement relation holds for spherical indentation on soft elastic solids undergoing large deformations. *Tribol Int* **97**: 71–76 (2016)
[70] Winkler E. *Theory of Elasticity and Strength*. Prague (Czechia): Dominicus, 1867 (in German)
[71] Fus N. An experience of theory on resistance by roads of various types to four-wheeled and two-wheeled carriages with definition of circumstances for which ones of these carriages are more useful than others. In: *Academic Papers Selected from the First Volume of "Activities of Academy of Sciences" under title Nova Acta Academiae Scientiarum Imperialis Petropolitanae*. Part 1: 373–422 (1801) (in Russian)
[72] Argatov I, Mishuris G. *Contact Mechanics of Articular Cartilage Layers: Asymptotic Models*. Cham (the Switzerland): Springer, 2015.
[73] Flanigan C M, Shull K R. Adhesive and elastic properties of thin gel layers. *Langmuir* **15**(15): 4966–4974 (1999)
[74] Perepelkin N V, Kovalev A E, Gorb S N, Borodich F M. Estimation of the elastic modulus and the work of adhesion of soft materials using the extended Borodich–Galanov (BG) method and depth sensing indentation. *Mech Mater* **129**: 198–213 (2019)
[75] Chu Y S, Dufour S, Thiery J P, Perez E, Pincet F. Johnson–Kendall–Roberts theory applied to living cells. *Phys Rev Lett* **94**(2): 028102 (2005)
[76] Lam C D, Park S. Nanomechanical characterization of soft nanomaterial using atomic force microscopy. *Mater Today Bio* **31**: 101506 (2025)
[77] Pedrolli L, Nadimi S, Achiaga B, López A. Estimation of mesoscale surface energy in the kinetic adhesion test. *Powder Technol* **435**: 119426 (2024)
[78] Ebenstein D M, Wahl K J. A comparison of JKR-based methods to analyze quasi-static and dynamic indentation force curves. *J Colloid Interf Sci* **298**(2): 652–662 (2006)
[79] Efremov Y M, Bagrov D V, Kirpichnikov M P, Shaitan K V. Application of the Johnson–Kendall–Roberts model in AFM-based mechanical measurements on cells and gel. *Colloid Surface B* **134**: 131–139 (2015)
[80] Borodich F M, Galanov B A. Non-direct estimations of adhesive and elastic properties of materials by depth-sensing indentation. *P Roy Soc A* **464**(2098): 2759–2776 (2008)
[81] Perepelkin N V, Borodich F M, Kovalev A E, Gorb S N. Depth-sensing indentation as a micro- and nanomechanical approach to characterization of mechanical properties of soft, biological, and biomimetic materials. *Nanomaterials* **10**(1): 15 (2020)
[82] Borodich F M, Galanov B A, Gorb S N, Perepelkin N V. Identification of adhesive and elastic parameters of materials by depth-sensing indentation. In: *Tribology Across Scales: Theory, Simulation and Experiment*. Starčević J, Heß M, Eds. Cham (the Switzerland): Springer, 2025: 25–47.
[83] Sirghi L, Rossi F. Adhesion and elasticity in nanoscale indentation. *Appl Phys Lett* **89**(24): 243118 (2006)
[84] Baqain S, Borodich F M, Brousseau E. Characterization of an AFM tip bluntness using indentation of soft materials. In: *Contact Problems for Soft, Biological and Bioinspired Materials*. Borodich F M, Jin X, Eds. Cham (the Switzerland): Springer International Publishing, 2022: 221–242
[85] Zhang X J, Zhang X H, Wen S Z. Finite element modeling of the nano-scale adhesive contact and the geometry-based pull-off force. *Tribol Lett* **41**(1): 65–72 (2011)
[86] Kadin Y, Kligerman Y, Etsion I. Jump-in induced plastic yield onset of approaching microcontacts in the presence of adhesion. *J Appl Phys* **103**: 013513 (2008)
[87] Hastie T, Tibshirani R, Friedman J. *The Elements of Statistical Learning*. New York (USA): Springer, 2009
[88] Green P J, Silverman B W. *Nonparametric Regression and Generalized Linear Models: A Roughness Penalty Approach*. Boca Raton (USA): Chapman and Hall/CRC, 1994.

Zhizhen Jiang obtained his bachelor degree in mechanical design, manufacturing, and automation from Yanshan University, China, in 2020. He is currently a Ph.D. student at Chongqing University, China. His research interests include contact mechanics and micromechanics.

Feodor M. Borodich is currently a professor and Hongshen distinguished scholar in College of Aerospace Engineering, Chongqing University, China. Before that he was a professor in School of Engineering, Cardiff University, UK. He was awarded by M.Sc. (1979), Ph.D. (1984), and D.Sc. (1990) degrees by Faculty of Mechanics and Mathematics of Lomonosov Moscow State University, USSR. He was also awarded by Diploma with distinction in civil engineering (1985) in Moscow, Russia, and by Honorary Doctor of Science degree (2016) of V.A. Belyi Metal-Polymer Research Institute, National Academy of Sciences of Belarus, Republic of Belarus. He is a Fellow of the European Academy of Sciences (2026) and a Foreign Member of the Russian Academy of Natural Sciences (2018). His current research interests are in nanotribology, nanoindentation, mechanics of adhesive contact and biomechanics.

Nikolay V. Perepelkin has more than 17 years of work experience in higher education. Nikolay is currently a senior lecturer at Leeds Beckett University, Leeds, UK. His preceding employment includes a postdoctoral researcher position at Cardiff University, Cardiff, UK. Nikolay holds his M.Sc. degree in mechanical engineering (2008) and his Ph.D. degree in mechanics (2013). His current research interests include the methods of mathematical modelling of materials and structures, particularly in relation to contact mechanics and tribology, using both analytical and numerical approaches. Previously, he has published a number of works in the area of nonlinear dynamics.

Xiaoqing Jin received his Ph.D. degree in theoretical and applied mechanics from Northwestern University, USA, in 2006, and then worked with Prof. Q. Jane Wang as a postdoctoral researcher. In February 2013, he was employed as a research professor in the State Key Laboratory of Mechanical Transmissions at Chongqing University, China. He has served as the department chair of Engineering Mechanics in the College of Aerospace Engineering at Chongqing University. His current research interests are in fracture and fatigue, contact mechanics, tribology and micromechanics, etc.